Shahrood University of Technology
Iranian Society of Mining Engineering (IRSME)
Journal of Mining and Environment (JME)
journal homepage: www.jme.shahroodut.ac.ir
THOMSON REUTERS
Vol. 10, No. 4, 2019, 883-901.
DOI: 10.22044/jme.2019.7948.1663

Delineation of alteration zones based on artificial neural networks and concentration-volume fractal methods in the hypogene zone of porphyry copper-gold deposit, Masjed-Daghi, East Azerbaijan Province, Iran

H. Nikoogoftar and A. Hezarkhani*

Department of Mining and Metallurgy Engineering, Amirkabir University of Technology (Tehran Polytechnic), Tehran, Iran

Received 7 January 2019; received in revised form 24 June 2019; accepted 29 June 2019

Keywords

Alteration Zones

Artificial Neural Networks

Concentration- Volume Fractal Model

Masjed-Daghi Porphyry Copper Deposit

Ordinary Kriging

Abstract

In this paper, we aim to achieve two specific objectives. The first one is to examine the applicability of the Artificial Neural Networks (ANNs) technique in ore grade estimation. Different training algorithms and numbers of hidden neurons are applied to estimate Cu grade of borehole data in the hypogene zone of porphyry copper-gold deposit, Masjed-Daghi, East Azerbaijan Province (Iran). The efficacy of ANNs in function-learning and estimation is compared with ordinary kriging (OK). As the kriging algorithms smooth the data, their applicability in the pre-processing of data for fractal analysis is not conducive. ANNs can be introduced as an alternative for this kind of problem. Secondly, we aim to delineate the potassic and phyllic alteration regions in the hypogene zone of Cu-Au porphyry deposit based on the estimation obtained by the ANNs and OK methods, and utilize the Concentration-Volume (C-V) fractal model. In this regard, at first, C-V log-log is generated based on the ANN results. The plots are then used to determine the Cu threshold values for the alteration zones. To investigate the correlation between the geological model and C-V fractal results, the log ratio matrix is applied. The results obtained show that Cu values less than 0.38% from ANNs have more overlapped voxels with phyllic alteration zone by an overall accuracy of 0.72. Spatial correlation between the potassic alteration zones resulting from 3D geological modeling and high concentration zones in C-V fractal model show that Cu values greater than 0.38% have more voxels overlapped with the potassic alteration zone by an overall accuracy of 0.76. Generally, the results obtained show that a combination of the ANNs and C-V fractal methods can be a suitable and robust tool for quantitative modeling of alteration zones instead of the qualitative methods.

1. Introduction

Porphyry copper deposits are usually generated in the process of cooling, depressurization, and reaction between the hydrothermal fluids and the wall (host) rocks causing assemblage of different alterations, and consequently, different grade distribution in each of them. In other words, grade distribution is related to alteration gradient [1-3]. As each alteration has specific geochemical, mineralogical, and petrological characteristics, their delineating can be useful in geo-metallurgy, mineral processing, and mine planning [4-9].

In the past few decades, many attempts have been made to achieve a reliable model of ore grade distribution. At the beginning, the conventional methods such as core drilling combined with chemical analysis would be applied to achieve an ore grade model. However, too much core drilling without considering the spatial dependency is expensive and time-consuming. Therefore, geostatistical techniques were introduced, which were based upon spatial relationships between the sample locations and the sample components in space. Also the underlying assumption of

* Corresponding author: ardehez@aut.ac.ir (A. Hezarkhani).

geostatistics (mean and covariance) is stationary [10-12]. Using geostatistics for spatial modeling of resource heterogeneities, predicting spatial attributes, and assessing uncertainty in reservoir forecasting has increased significantly since the 1990s [13-18].

Over the past 50 years, many researchers have used various geostatistical methods such as simple kriging, Ordinary Kriging (OK), lognormal kriging, indicator kriging, co-kriging, universal kriging, residual kriging, moving window regression residual kriging, disjunctive kriging, and stochastic simulation such as Sequential Gaussian Simulation (SGS) and Sequential Indicator Simulation (SIS) in ore grade modeling. Kriging, as a group of geostatistical methods, is an interpolation technique that considers both the degree of variation and the distance between known data points in estimating the values in unknown areas [19-32]. In geostatistical simulation, reproduction of statistics and spatial variability takes precedence over local accuracy [33, 34].

Despite the widespread application of geostatistical methods, they suffer from some limitations: (1) they are based upon certain stationary assumptions like being a second-order stationary random field with an unknown constant mean; (2) they use a linear correlation between any two points in space; (3) they require abundant data to be processed, which restricts their learning and efficient application; and (4) they require deep mathematical thinking and skills and taking too much time to get the preferred solution [10, 26, 30].

Due to the aforementioned problems, many research works have been conducted to inspire from nature. One of the methods inspired from nature is Artificial Neural Networks (ANNs). Over the years, various types of ANNs have been used in the geoscience field [35-40]. ANNs have shown a great importance in mining engineering due to their capability to analyze complex and non-linear problems. In the neural network diagrams, ore grade variability is considered as non-linear input–output mapper of a set of connection weights. ANNs seems to work like a parametric non-linear global fitting model, while geostatistics methods work as non-parametric local fitting models that restrict the fit of the model to a local data point neighborhood. Hence, ANNs is expected to provide improved performance in the presence of a non-linear spatial trend in the data variability [41]. Furthermore, ANNs, unlike the geostatistical methods and techniques, is not based on the assumption of stationary. Regarding the mentioned advantages along with the high accuracy, ANNs is an appropriate alternative for the conventional methods [30].

In addition, fractal and multi-fractal theories based on the drill core data can provide quantitative modeling for determining alteration zones in the porphyry deposits. The fractal geometry is specifically able to discern the natural populations as several ore grades within a deposit [42]. The fractal theory introduced by Mandelbrot (1983) became an important tool for studying non-linear and complex sciences [43]. Fractal/multi-fractal modeling has been a powerful tool in geoscience for identifying anomalies [44, 45], evaluating the vertical distribution of geochemical data [46 47], image processing of the satellite information [48, 49], and characterizing the properties of mineralization and mineral deposits. There are different types of fractal and multi-fractal models such as the concentration-area [50], concentration-distance [51], power spectrum-area [52], concentration-number [53], and concentration-volume models [42], which have been reported in processing the earth science data.

In this work, ANNs and OK were applied to estimate cu grade in a hypogene zone. After comparing the results obtained, ANNs and C-V fractal modeling were used to delineate the alteration regions in the hypogene zone of the porphyry ore deposit in the Masjed-Daghi district, NW Iran.

This article is organized as what follows. In section 2, the case study is investigated from the aspects of regional geology, structural geology, and geological setting. An overview of principles, advantages, and limitations of the methods are drawn in Section 3. In Section 4, the borehole dataset and statistical calculations are described. The results are discussed in Section 5. Finally, conclusions are presented in Section 6.

2. Case study

There are many structural and lithotectonical zones in Iran [54] that are generally divided into the following categories: i) Zagros, ii) Sanandaj-Sirjan, iii) Sahand-Bazman, iv) Central Iran, v) Alborz, vi) Kope Dagh, vii) Lut block, vii) Makran, and ix) East-Iranian suture zone. The Urumieh-Dokhtar Magmatic orogenic zone, formed as a result of subduction of the Arabian plate beneath central Iran during the Alpine orogeny, hosts all the known Iranian porphyry

copper mineralizations (Figure 1) such as the Sar-Cheshmeh and Sungun deposits [54].

The copper-gold deposit of Masjed-Daghi area is located in the east Azarbaijan Province, NW Iran. The Masjed-Daghi area, as a part of Alborz-Azerbaijan zone, is in the 1:100,000 geological sheet [55, 56]. The oldest rock units that have been cropped out widely in the south and SE of the area belong to the Eocene flysch-type sediments. The outcropped rocks including andesite, trachyandesite, and quartz mostly result from tertiary volcanic and volcano-sedimentary activities, which have affected the region and intersected by late Eocene intrusive [55, 56]. The mineralographical studies have shown that the mineralization in the area is of copper sulfide type in the form of veins, veinlets, and stock works. Pyrite has been mostly observed alongside the depth relative increasing amounts of chalcopyrite and chalco-pyrrhotite. The paragenetic observations of the gangue and alteration surrounding the veins indicate the presence of the gold-bearing epithermal veins with a high sulfide content. The occurrence of the native gold mineralization has been observed in the siliceous zone and in the form of inclusions in the host rock of the veins (about 15 microns) in chalcopyrite. This phenomenon has been reported for the first time in this area. The lead and zinc mineralizations exist in the body of the vein but not in the altered zone. Moreover, a very small amount of molybdenite is present adjacent to the veins and stock works. The existing alteration types in the area are potassic, phyllic, carbonate-phyllic, argillic, and propylitic. Furthermore, selective sericite, sericite-chlorite, and alunite alterations have been observed around the mineralized veins [57].

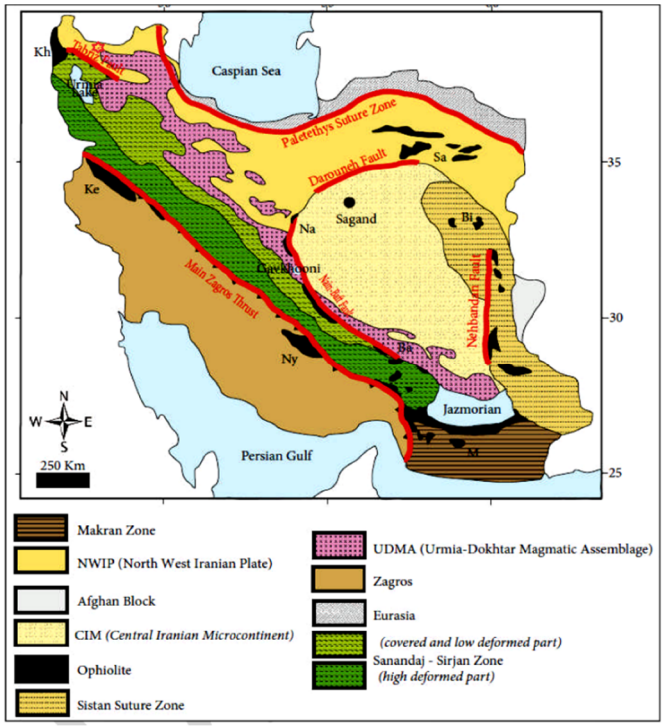

Figure 1. The structural map of Iran (corrected after [56]).

2.1. Geology and lithology of studied area

The studied area is located in the Central Iran geological zone regarding Stoecklin (1968), and is considered as a part of the West Alborz zone called Alborz-Azerbaijan zone regarding Nabavi (1976) and Eftekharnejad (1980). According to the geology, the area is known to be a part of the Ahar mineralization, and confined by the Tabriz-Soltanieh fault in the south and SW, Ardabil-Mianeh fault in the east, and by the EW fault of Moghan [57] in NE.

Volcanic activity in the area started from the upper cretaceous era marine facies and reached its peak in the middle Eocene with Marine-land facies. In the upper Eocene-Oligocene era, igneous activities have been plutonism, and in the neogene era, these activities have continued as shallow intrusive bodies of dacite-rhiodacite, trachyte, and andesite and basaltic trachyte.

The effects of volcanism in this area could be observed in the form of Andesite trachy domes (Masjed-Daghi heights), which led to the crushing of the older rocks (Eocene Flysch). These domes

include andesite, trachy andesite, quartz, and quartz lattice. The boundary between the altered trachy andesites and the andesitic lava is not easily detectable. According to the petrographic studies, the texture of the rocks are porphyric microlyte and microgranular with a microcrystalline matrix. The main minerals include shaped and non-shaped plagioclase and have been degraded by the alteration to the clay and sericitic minerals. Occasionally, delicate fractures have been observed in the feldspars that are filled with pyrite, chlorite, epidote, and iron oxides. Ferromanganese minerals have also been decomposed and converted to the iron oxides, calcite, and chlorite. The main factor of the hydrothermal alteration and mineralization in the studied area is the intrusive bodies. The main combination of these rocks is known as quartz-monzonite. Their color is bright, and their texture is porphyritic with micro-granular matrix. The main mineral is quartz (Figure 2) [55, 56].

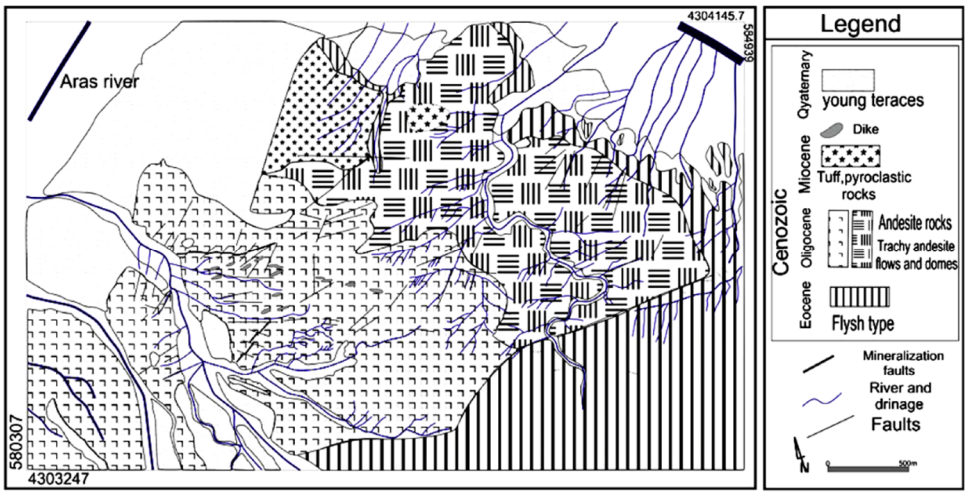

Figure 2. Geological map of Masjed–Daghi area in the scale of 1:5,000 [56].

2.2. Alteration

The dominant alteration in the studied area is of the argillic type, which often affects the rocks, especially the trachyandesite and diorite. Other alterations in the area are potassic, phyllic, and silica. The most important alteration products in the studied area are Argillic alterations, which are gradually converted to sericitic alteration and cover a wide part of the trachyandesite rocks. Based on the petrography studies, mafic minerals (amphibole) have been decomposed into a series of chlorite, calcite and clays, sericite, and epidote, and feldspar (plagioclase) minerals have also been completely decomposed into a set of carbonate, sericite, jarocite, alunite, and hematite minerals in these specimens. The Argillic alteration intensity is very strong, and only the shape of the early minerals have remained in this alteration. The results of XRD studies showed the presence of abundant clay minerals such as jarocite, pyrophyllite, kaolinite, and alunite. In addition, based on the results of mineralogy studies, minerals such as pyrite, chalcopyrite, Sphalerite, and rutile exist in this region [57].

The Potassic alteration zone in the studied area shows a small outcrop in the Arpachay region. The studied samples, however, show fine-grain and amorphous alkaline feldspars, which are decomposed into clay minerals. In this area, the rocks that consist of andesite and trachyandesite are affected by the phyllic alteration. Moreover, plagioclase is completely altered to carbonate and chlorite, and the mafic minerals (amphibole) have been converted to muscovite and sericite. The primary biotite in this zone is decomposed into chlorite, muscovite, and oxide minerals. The presence of pyrite in the alteration zone is an evidence of crystal conversion to hydrophilic oxides and secondary iron oxides. In some samples, concentrations of carbonate are found in the matrix of the rock. Yet, carbonate sometimes has been observed as veins and veinlets. Therefore, this zone is divided into two parts, phyllic and phyllic carbonate [57].

Silica alteration around the mineralized veins is high in the form of veinlets in the dacite of the area, which is an appropriate environment for the mineralization of gold. High amounts of silica in the region are considered as an indicator of the hydrothermal solution saturation from silica after hydrothermal alteration. The mineralization of samples in this altered zone shows the minerals of

pyrite, chalcopyrite, and marcasite. The samples that are taken and analyzed from the trenches indicate a high concentration of gold, which is directly related to silicification.
Propylitic alteration has been observed in the andesitic volcanic rocks and margin of siliceous veins. One of the most significant indicators of this alteration is the presence of the epidote, which is in green color along with chlorite. This green band is observed on the edge of the andesites. Gold mineralization concentrates are highly in the propylitic alteration due to the presence of zirconia, barite, and quartz-containing veins [57].

2.3. Mineralization

The most significant forms of mineralization in the Masjed-Daghi area are the rutile, magnetite, pyrite, chalcopyrite, calcopyrotit, bornite, sphalerite, covillite, and chalcocite minerals. The last two minerals have been formed as secondary crystals of the alteration in the region. In the Masjed-Daghi area, mineralization of gold, lead, and zinc has been formed along with the siliceous-barite veins. Molybdenum mineralization is associated with the vein deposits and copper stock works. Along with this mineralization, there are also tin and tungsten traces. Gold mineralization in this area can be observed in both the epithermal and the copper mineralizations [57].

3. Methods

3.1. Ordinary kriging (OK)

Over the past few decades, different spatial interpolation methods have been presented by numerous researchers. However, most of them are related together and have similar principles. Spatial interpolation models can be categorized into two classes: (a) mechanical/deterministic and (b) statistical/probability groups. The mechanical models are based upon empirical model parameters, which include techniques like Inverse Distance Weighting (IDW) and Splines. They do not consider the error estimation. In contrast, the parameters of the statistical/probability techniques are estimated based on the probability principles and consider the error estimation. One of the most important statistical/probability models is kriging, which is based on the"Theory of Regionalized Variables" [58, 59]. The technique was first introduced by Krige (1951) but in 1963, G. Matheron derived the formulas and founded the linear geostatistics [60, 61]. The kriging technique, which is commonly known as a 'minimum variance estimator', consisting of two basic steps. The first is an estimation of the semi-variogram using sample data, given by:

$$\gamma(h)=\frac{1}{2.n(h)}\sum_{i=1}^{n(h)}\{z(i)-z(i+h)\}^2 \quad (1)$$

where $\gamma(h)$ is the estimate of semi-variance, n(h) is the number of pairs observed [z(i), z(i+h)], and h is the distance between the pairs.
The second is predicting the value at unknown spatial coordinates through a linear combination of measured values shown by:

$$z^*(x_0)=\sum_{i=1}^{n}\lambda_i.z(x_i) \quad (2)$$

where $z^*(x_0)$ is the estimated value for any location x_0, n is the number of measured value z(i), $z(x_i)$ is the value involved in the estimation, and $)\lambda_i$ is the weight attached to each measured value z(i).
The best estimator is always unbiased and has a minimum variance. Therefore, the kriging system can be deduced as:

$$\sum_{j=1}^{n}\lambda_j.\gamma(x_i,x_j)=\mu+\gamma(x_i,x_0) \quad (3)$$

where $\gamma(x_i, x_0)$ is the semi-variance function of a vector with an origin at x_i and extremity at x_0; $\gamma(x_i, x_j)$ is the semi-variance function of a vector with an origin at x_i and extremity at x_j; and μ is the Lagrangian multiplier [59].
OK is an appropriate geostatistical estimator and the most useful technique among the different kriging methods [59, 62]. OK, as a linear estimation method, assigns weights to the sample locations inside the estimation neighborhood, which are independent from the data values at these locations. OK is a moving average method satisfying the different types of data dispersion, e.g. sparse sampling points [63-65]. The technique minimizes the conditional bias and estimation variance for each single estimate at each location [61, 66]. Most of the theories about OK rely on the work of Georges Matheron (1963), and have been developed by some others [67-71].
In mathematical terms, OK is a spatial interpolation estimator $z^\wedge(x_0)$ that is used to find the best linear unbiased estimate of a second-order stationary random field with an unknown constant mean, as follows:

$$z^\wedge(x_0)=\sum_{i=1}^{n}\lambda_i.z(x_i) \quad (4)$$

where $z^{(x_0)}$ = kriging estimate at a non-sampled location x_0; $Z(x_0)$ = sampled value at location x_i; and λ_i = weighting factor for $Z(x_i)$.
The estimation error is:

$$z^{(x_0)} - z(x_0) = R(x_0) = \sum_{i=1}^{N} \lambda_i . z(x_i) - z(x_0) \quad (5)$$

where $Z(x_0)$ = unknown true value at x_0; and $R(x_0)$ = estimation error. For an unbiased estimator, the mean of the estimation error must equal zero.
Therefore:

$$E\{R(x_0)\} = 0 \quad (6)$$

and

$$\sum_{i=1}^{N} \lambda_i = 1 \quad (7)$$

A minimum variance of estimation error is required for solving the interpolation problem by kriging [62-64, 69, 70].

3.2. Artificial Neural networks (ANNs)

A very powerful method that has attracted the attention of the researchers over the past few decades is ANNs, which has been used for ore grade modeling [72]. ANNs has a non-linear mathematical structure that is able to perform any curve-fitting operation in a multi-dimensional space. Hence, it is able to represent an arbitrarily complex data generating a process that links the inputs and outputs of that process [73].
In ore grade modeling/estimation, it is supposed that the attributed grade value in an ore deposit varies from one location to another, and this will be reflected in a complex input and output spatial relationship between grade values and spatial coordinates in the area of interest. Therefore, the output grade is considered to be a function of spatial coordinates like X, Y, and Z [74, 75].
There are many ANNs types such as feed-forward neural network, Radial Basis Function (RBF) network, and Kohonen self-organizing network [76]. Three major components are particularly important in every ANNs system: (a) structure of the nodes, (b) topology of the network, and (c) learning algorithm used to find the weights of the ANNs.
On the other hand, in an ANNs, each processing unit acts as an idealized neuron, receives input, computes activation, and transmits that activation to other processing units. A weight value, defined to represent the connection strength, is associated with each connection between these processing units. The connection weight of each processing unit is optimally determined through the presentation of known examples, and application of a learning rule. Once the connection weight is determined through NN learning, the inter-connection between input and output embedded in the data is captured [77].
An architecture of ANNs with a sigmoid activation function is presented in Figure 3.

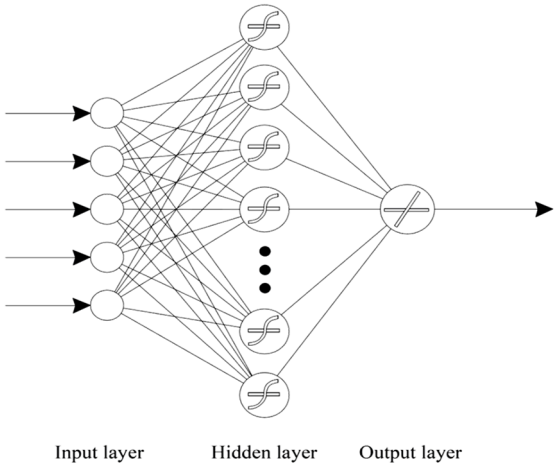

Figure 3. Architecture of ANNs with sigmoid activation function.

It contains an input layer, a hidden layer, and one output layer, which are connected by modifiable weights and represented by links between the layers. Each input vector is presented as the input layer, and the output of each input unit equals the corresponding elements in the vector. Each hidden unit computes the weighted sum of its input to form its net activation [78]. The above-mentioned subjects can be expressed in mathematical terms by Eq. (8):

$$net_j = \sum_{i=1}^{d} x_i w_{ij} + w_{j0} = \sum_{i=0}^{d} x_i w_{ij} \quad (8)$$

where the subscripts i and j are indexed units in the input and hidden layers, respectively, W_{ij} denotes the input to the hidden layer weights at the hidden unit j, and net j is the activation for hidden j. Each hidden unit emits an output that is a non-linear function of its activation, f(net), in the form of Eq. (9):

$$y_j = f(net_j) \quad (9)$$

Each output unit similarly computes its net activation based on the hidden unit signals as Eq. (10):

$$net_k = \sum_{j=1}^{n_H} y_j w_{kj} + w_{k0} = \sum_{j=0}^{n_H} y_j w_{kj} \quad (10)$$

where the subscript k indexes the units in the output layer and n_H denotes the number of hidden units. An output unit computes the non-linear function of its net, as Eq. (11):

$$z_k = f(net_k) \quad (11)$$

where z_k is the k output unit. Therefore, the total network output for a three-layer model can be calculated in the form of Eq. (12) [74]:

$$z_k = f(\sum_{j=1}^{n_H} w_{kj} f(\sum_{i=1}^{d} w_{ji} x_i + w_{j0}) + w_{k0}) \quad (12)$$

3.3. Concentration-volume (C-V) fractal model

The C-V fractal modeling, which was first proposed by Afzal *et al*. (2011) for identification of different mineralization zones in porphyry Cu deposits, can be generally expressed as Eq. (13) [42, 79, 80]:

$$V(\rho \le \upsilon) \propto r^{-a_1}; V(\rho \ge \upsilon) \propto r^{-a_2} \quad (13)$$

where $V(\rho \le \upsilon)$ and $V(\rho \ge \upsilon)$ represent the volumes with concentration values (ρ) less than or equal to and greater than or equal to the contour values (υ); and a_1 and a_2 are the characteristic exponents. The contour value (υ) in this model explains the boundaries that separate various mineralized (alteration) zones and concentration populations. In this work, the OK and ANNs outputs (block model) were processed by the C-V fractal method, and $V(\rho \le \upsilon)$ and $V(\rho \ge \upsilon)$ (the volumes enclosed by a concentration contour) were calculated in a 3D space [42].

4. Borehole dataset

The borehole dataset plays an important role in geoscience investigations in both the mineral exploration and grade estimation. A total of 50 boreholes were drilled in the studied area in which, 16 of them belonged to the pre-drilled boreholes (BH series) with a total length of 1882.3 m and 34 boreholes were related to MAD series with a total length of 15015.95 m (Figure 4). The dataset included the collars, lithology, down-hole survey, and assay. The other acquired data was zone, alteration, mineral, and recovery. The dataset for assay was analyzed by the ICP-MS method at the Zarazma laboratory, Tehran. Based on the mineralogical, geological, and geochemical results, it was found that the case study was favorable for the mineralization of Cu. The data was validated and subjected to statistical analysis. The histogram, Q-Q plot, and descriptive statistics of the copper grades from 8267 samples in the hypogene zone of the case study are shown in Figure 5 and Table 1. The statistical parameters of Cu grade based on the alteration in the hypogene zone of the case study are also shown in Table 2. Accordingly, two alteration zones composed of potassic and phyllic accounted for more than 90% of the data length. The Cu regionalized variable was modeled by a second-order stationary random function. There was no trend of Cu concentration in any direction; this means that Cu concentration does not depend on the coordinates of the samples (Figure 6 (a-c)). Consequently, assumptions of the stationary are tenable.

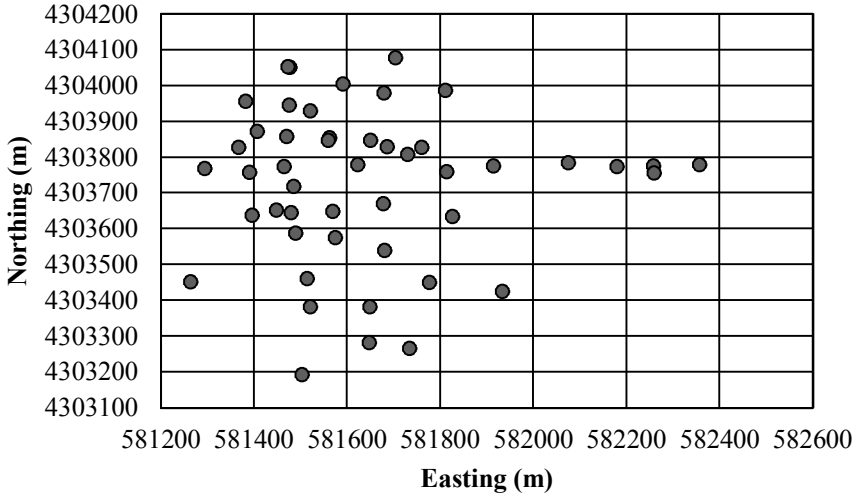

Figure 4. Borehole location map of the studied Cu porphyry deposit.

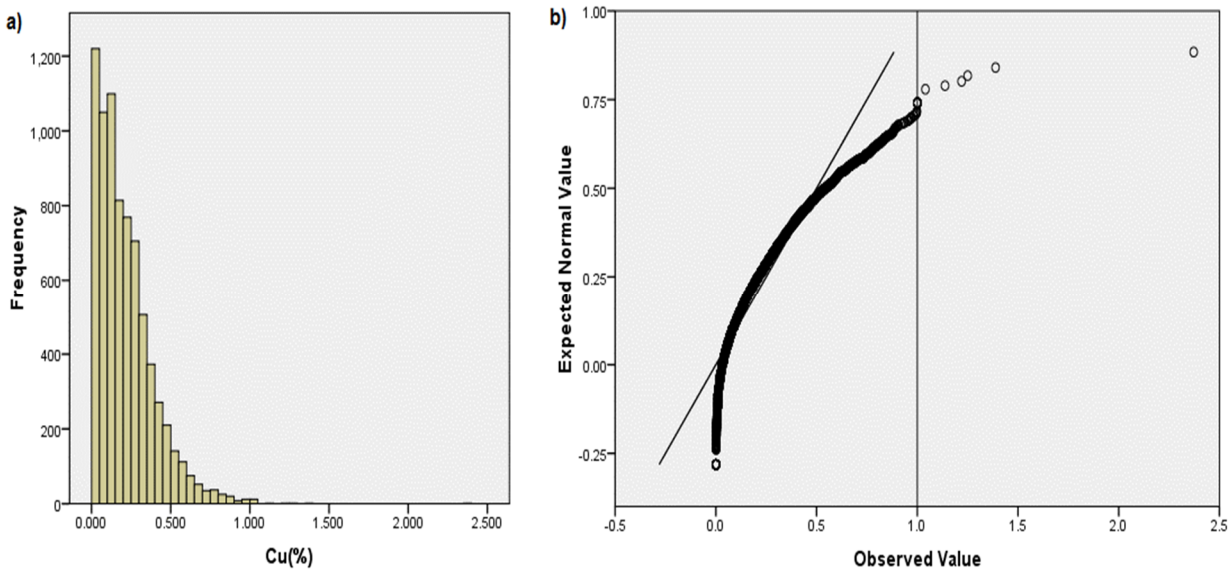

Figure 5. a) Histogram of the Cu raw data and b) Q-Q plot of the Cu data in the hypogene zone of Masjed-Daghi deposit.

Table 1. Statistical parameters of the Cu element in the boreholes (raw data).

Variable	Length (m)	Mean	Minimum	Maximum	Std. Deviation	Variance	Skewness
Cu (%)	15952	0.643	0.001	4.8	0.480	0.231	1.011

Table 2. Statistical parameters of the Cu grade based on the alteration in the hypogene zone.

Alteration type	Length	Length%	Cu		
			Min.	Max.	Mean
ARG	84.3	0.49	0.072	0.784	0.325
CHL	44	0.26	0.02	0.1	0.058
NA	1151.45	6.81	0	1.22	0.15
PHY	**3705.9**	**21.93**	**0**	**1.04**	**0.158**
POT	**9847.45**	**58.32**	**0**	**1.38**	**0.248**
PRP	16.1	0.09	0.009	0.023	0.0137
SER	8.4	0.04	0.181	0.419	1.246
SLC	158.35	0.93	0.007	0.93	0.134

ARG = Argillic; CAL = Calcified; CHL = Chloritic; PHY = Phyllic; POT = Potassic; PRP = Propylitic; SLC = Silicified; and NA = Not Applicable.

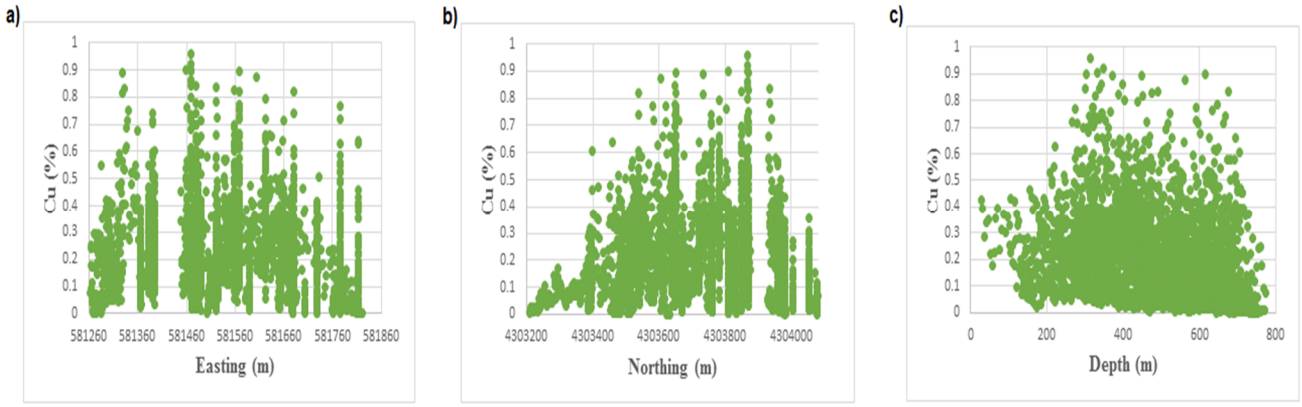

Figure 6. Variability of Cu concentration in a) east-west direction, b) north-south direction and c) depth within the hypogene zone of Masjed-Daghi deposit

5. Results and discussion

5.1. OK results

Here, the data in Section 3 is used to estimate the Cu grade. However, prior to the kriging calculations, it is necessary to carry out a series of data pre-processing. The first step is to determine and correct the outlier values. These values dramatically impact the statistical analysis and result interpretation. High-grade values as outliers are able to transform a mineral occurrence into an economic mineral deposit, and may be sufficient to justify the development of a mining project [81, 82]. There are several ways to deal with the effects of the outlier values and control them. In this work, the box plot (Figure 7) is applied to remove the outlier values [83]. Another important issue in the pre-processing is the composite data. In other words, it is very important to work with equal volume samples [84]. In this work, the data for the analysis of Masjed-Daghi reservoir using the OK method is divided into 2 m composites. According to the composite length, the lowest loss length is obtained, while the Cu grade and variance of Cu are similar to the original data.

Data variography for OK is the next step after data pre-processing. Given the spatial variability and randomness, the variogram function can reflect the structure of the spatial variability of the regional variable. The best way to describe the spatial dependencies in the process of stationary is covariance variogram.

Since mineralization does not have the same behavior in each direction, it will be anisotropic. Consequently, in order to determine the spatial structure correctly, it is necessary to perform a single analysis in several directions. As the experimental variograms show different behaviors in different directions, the anisotropic variogram model should be fitted to them. In general, the variogram has orientational properties in a more than one direction. In this work, the variogram was performed using the high-power Datamine software.

An omni-directional semi-variogram of raw data along azimuth of 00°, Plunge of 00°, spread of 90°, and lag spacing of 40 m follows a spherical model with a nugget effect of 0.052 $(\%)^2$, which reaches a sill of 0.02 $(\%)^2$ at a range of 204 m (Figure 8-a). To investigate anisotropy, directional semi-variograms are thereafter calculated and modelled in different directions with 30°horizontal angular increments, 15°horizontal angular tolerance, 30°vertical angular increments, and 15°vertical angular tolerance in the hypogene zone of the porphyry ore deposit. Because of the different ranges of variograms, the ore deposit has anisotropy. The main resulting directions from variography for the three principal directions of the search ellipsoid are presented in Figure 8 (b)-(d). The directional semi-variogram model parameters are shown in Table 3.

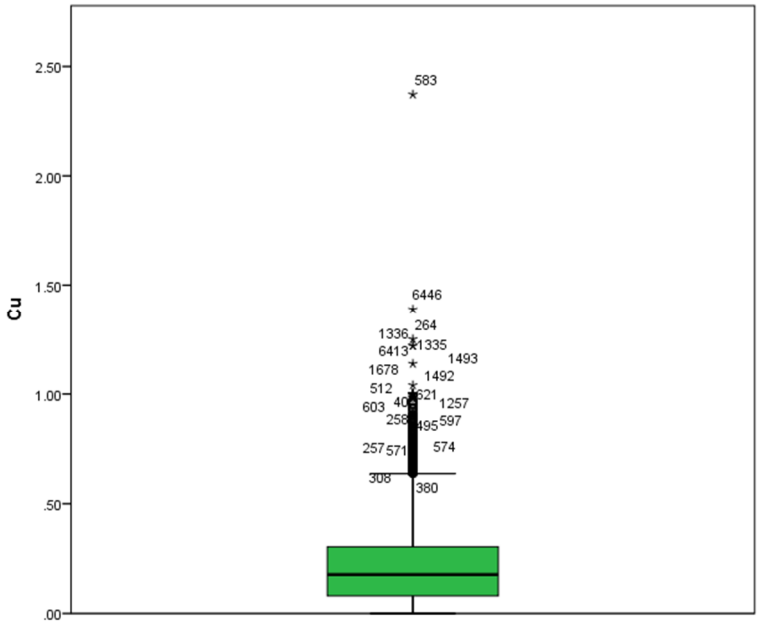

Figure 7. The box plot used to remove the outlier data.

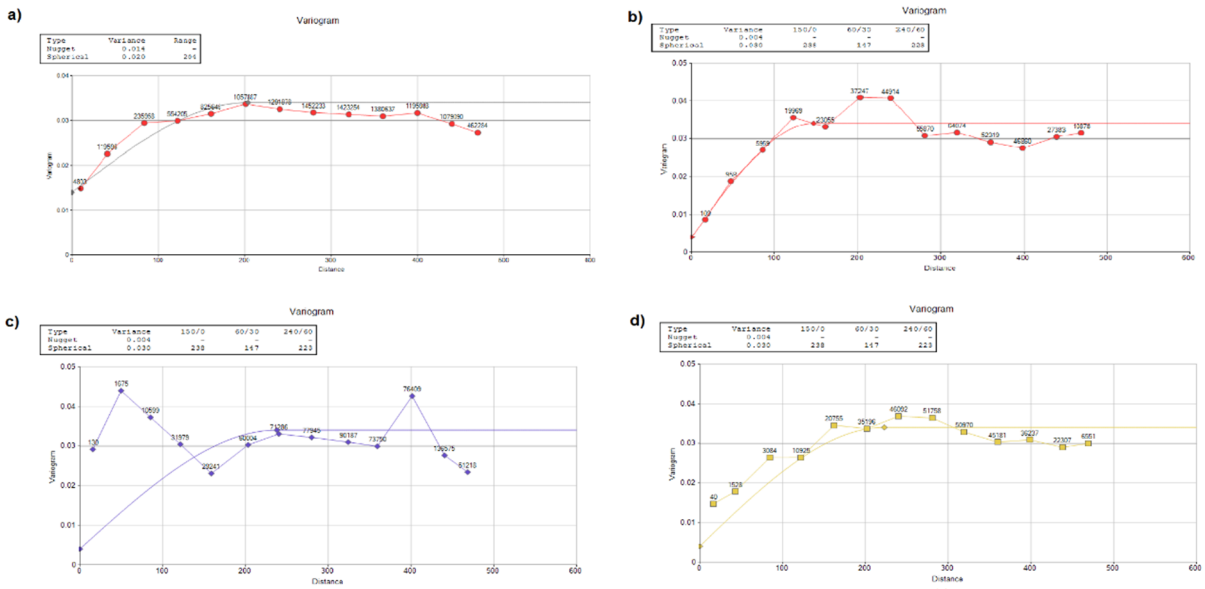

Figure 8. Experimental semi-variogram and appropriate fitted model of the (a) omnidirectional semi-variograms and (b) directional semi-variograms with Azimuth = 60; Dip = 30 (c) directional semi-variograms with Azimuth = 150; Dip = 0 (d) directional semi-variograms with Azimuth = 240; Dip = 0 for the 3 main directions of the search ellipsoid in the hypogene zone of Masjed-Daghi porphyry ore deposit.

Table 3. Directional Semi-variogram parameters for three principal directions of the search ellipsoid in the hypogene zone of the porphyry ore deposit.

Variogram model	Azimuth	Dip	nugget effect $(\%)^2$	Range (m)	Threshold $(\%)^2$
Spherical	60	30	0.004	147	0.03
Spherical	150	00	0.004	238	0.03
Spherical	240	60	0.004	223	0.03

The cross-validation method is used to validate the fitted model to the variogram of the hypogene zone. The correlation coefficient of the estimated values and actual values was partially acceptable and about 80%.

To confirm the practicality of OK in estimating the unsampled locations, this method was applied in the hypogene zone of the porphyry ore deposit. The estimation of Cu (%) is performed on a 10 × 10 × 10 m grid. The estimation and 3D modeling process are commenced from the elevation of 0 to 800 m above the sea level in the mine. It also began from 581113 to 582043 m in the east direction and from 4303279 to 4303279 m in the north direction. 3D modeling in the mineral deposit has many advantages. Therefore, if this process is carefully performed, evaluations and judgments on the different parts of the deposit will be more accurate. The 3D model of the Cu grade by OK in the Cu copper deposit is shown in Figure 9.

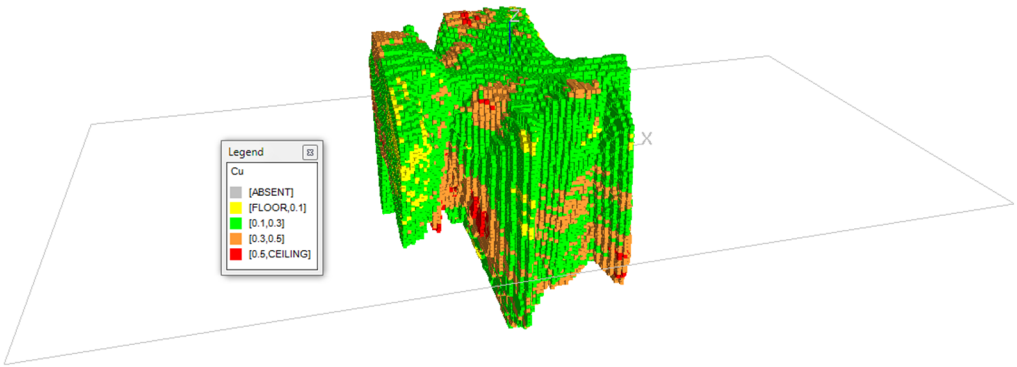

Figure 9. 3D model of Cu concentration estimation by OK.

5.2. ANN results

There are a lot of types of ANNs. The most popular and the best-known ANNs are feed forward neural network, Radial Basis Function (RBF) network, Kohonen self-organizing network, and modular neural networks. Generally, three elements are particularly important in every model of ANNs: the structure of the nodes, the topology of the network, and the learning algorithm used to find the weights of the network. The learning algorithm is an adaptive method by which a network of computing units organizes itself to implement the desired behavior. This is performed in some learning algorithms by presenting some examples of the desired input–output mapping of the network. In this work, instead of using complex ANNs like RBF and WNN, Multi-Layer Perceptron (MLP) with Levenberg–Marquardt (LM) and scaled gradient descent (SGD) algorithms are applied to estimate the Cu grade based on the borehole dataset. Although the network used in this work has a simple structure, the learning algorithm is powerful and sufficient for the purposes (a comparison between ANNs and OK for ore grade estimation) of this article. For modelling based on MLP, the following steps are followed.

5.2.1. Sample data acquisition

A sufficient amount of data is required for ore grade estimation in the train, validation, and test steps in ANNs. In this work, data on Masjed-Daghi porphyry copper deposit has been used. According to the available reports, the deposit is non-homogeneous. The applied values in the deposit are divided into blocks of 10 × 10 × 10 m. The borehole coordinates and actual grade were used as the input and output data for training, respectively. Figure 10 shows an example of the arrangement of the points that are utilized to estimate the central point from the surrounding data.

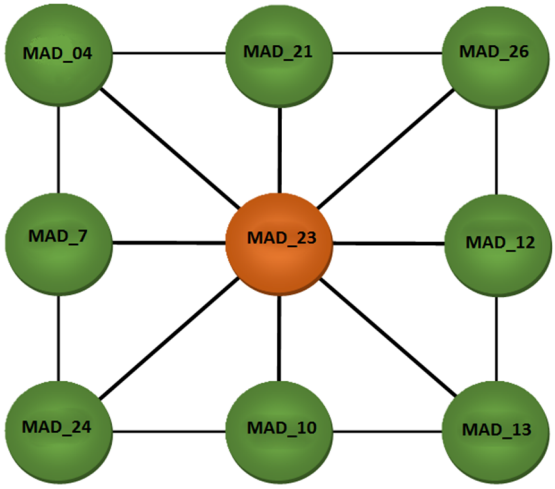

Figure 10. Input and output data arrangement.

5.2.2. Data preparation

Data pre-processing that is applied to train and validate the ANN topologies is discussed after selection of the source data deposits. At the first stage of the modeling, the data is normalized, which helps to scale the inputs and output, and consequently, leads to a better prediction [85, 86]. Different methods have been developed to improve the network training in data normalization. In this work, the input and output data is normalized by Eq. (14):

$$X_{norm} = \frac{x - x_{min}}{x_{max} - x_{min}} \quad (14)$$

where x is the data that should be normalized, and x_{max} and x_{min} are the maximum and minimum of the original data, respectively. Moreover, X_{norm} is the transformed normalized data.

Divisionism as one of the most important issues would lead to inaccurate and illogical results if it has not been considered properly. The ANNs data is divided into three groups: 1) training data, 2) testing data, and 3) validation data [87, 88]. In this work, at first, 5402 Cu data with 2 m composites are used for training, testing, and validation of ANNs; all the datasets are divided into three distinct subsets consisting of the training data (70%), testing (15%), and validation (15%). After training the neural network, the coordinates of the

block centers (90352 sample) were given as a new input to the neural network, and the amount of copper was estimated as the output.

5.2.3. Performance of ANNs

There are various indicators to evaluate the accuracy of the models [89]. A complete description of these indicators can be found in [90]. In this work, the coefficient of determination (R^2) and Root Mean Square Error (RMSE) are applied. The degree of correlation between the observed and predicted values as well as a model strength through developing a relationship between the input and output variables are measured by R^2. The values of R^2 range from 0 to 1, in which 1 indicates a perfect fit between the data and the line drawn through it, and 0 represents no statistical correlation between the data and the line. R^2 is calculated by Eq. (15) [91]:

$$R^2 = 1 - \frac{\sum_{k=1}^{N}(t_k - y_k)^2}{\sum_{k=1}^{N}(t_k - \bar{t}_k)^2} \quad (15)$$

where t_k and y_k are target and network outputs for the k_{th} output, respectively; $\bar{t}_k$ is the average of the targets, and N is the total number of the considered events.

RMSE indicates the difference between the observed and calculated values. The lower the RMSE, the more accurate is the prediction. RMSE is calculated by Eq. (16):

$$RMSE = \sqrt{\frac{\sum_{i=1}^{N}(y_i - \bar{y}_i)^2}{N}} \quad (16)$$

where y_i is the observed data, $\bar{y}_i$ is the calculated data and N is the number of observations.

5.2.4. Modeling of ANNs

As stated earlier, there is no clear linear relationship between the coordinates of the points and corresponding grades but the relation between them is non-linear and complex. In this work, the 2017 version of the MATLAB software was used for ANNs modeling. The ANNs model is based on a neural network of back-propagation with a hidden layer. The optimum number of the hidden layers was estimated to be 9 neurons by trial-and-error (Table 4). At the beginning, the back propagation method is implemented by the Levenberg–Marquardt (LM) and scaled gradient descent (SGD) algorithms. The sigmoid and linear functions are used for the hidden and output layers, respectively. The learning and momentum parameters that obtained the best results were estimated to be 0.05 and 0.7, respectively. An early stopping technique is applied to ensure that the network is not over-fitted. The 3D model of the Cu grade by the ANNs method for the Masjed-Daghi porphyry deposit is shown in Figure 11.

A comparison between the two methods ANN and OK showed that both methods were able to estimate Cu grade very well. The advantage of the ANNs method is that it does not require any pre-processing or need to carry out variogram operations. It also can be used for initial data without any special pre-processing. However, the OK algorithm smooths the data, and thus its application to pre-processing of data for fractal analysis is not suitable. In the next sub-section, the ANN results are used for the determination of alteration zones in the Masjed-Daghi porphyry copper-gold deposit.

Table 4. Results of the observed and predicted data obtained from ANNs. The best network obtained is in bold.

Number	Number of neurons in hidden layer	Training algorithm	Train			Test			Validation		
			R^2	SSE	RMSE	R^2	SSE	RMSE	R^2	SSE	RMSE
1	2	SCG	0.66	1.71	0.61	0.53	1.80	0.63	0.57	1.82	0.63
2	3	SCG	0.68	1.68	0.55	0.59	1.74	0.61	0.58	1.72	0.6
3	4	LM	0.72	1.62	0.51	0.64	1.73	0.54	0.73	1.61	0.57
4	5	LM	0.79	1.59	0.49	0.72	1.62	0.58	0.64	1.66	0.58
5	6	LM	0.81	1.54	0.44	0.73	1.63	0.56	0.78	1.55	0.54
6	7	LM	0.87	1.41	0.43	0.78	1.59	0.50	0.73	1.55	0.54
7	8	LM	0.89	1.37	0.39	0.81	1.49	0.48	0.84	1.59	0.59
8	**9**	**LM**	**0.93**	**1.24**	**0.37**	**0.88**	**1.14**	**0.35**	**0.89**	**1.56**	**0.54**
9	10	SCG	0.90	1.46	0.63	0.84	1.59	0.44	0.85	1.56	0.54
10	11	SCG	0.87	1.51	0.72	0.81	1.62	0.54	0.79	1.76	0.68

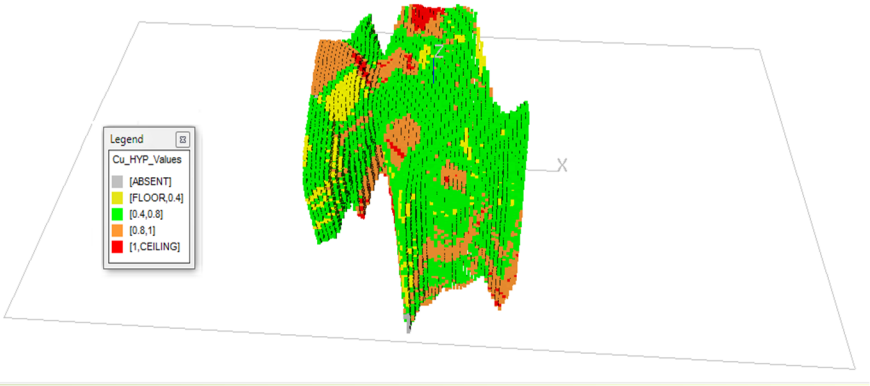

Figure 11. 3D model of the Cu concentration estimation by ANNs in the Mashhad-Daghi porphyry deposit.

5.3. Results of C-V fractal model

After grade estimation, the volume of each block is calculated in order to be used in the C-V fractal modeling. The C-V log-log plots show a power-law relationship between the copper contents and the volumes corresponding to them. Threshold values of Cu are identified in the C-V plots (Figure 12). According to this plot, a threshold value of 0.28 (%) Cu and two communities are obtained.

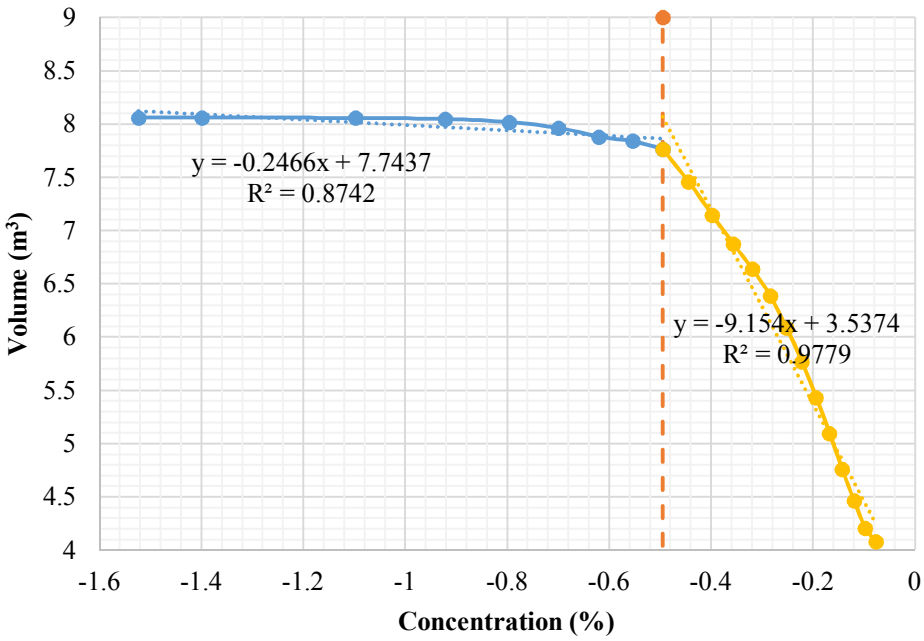

Figure 12. Log-Log plot of C-V fractal model based on the ANNs estimations.

5.4. Comparison between fractal and spatial alteration models

In order to validate the results obtained through the C-V fractal modeling, the models are compared with the 3D alteration zone models for the Masjed-Daghi porphyry copper deposit' zone comprising the phyllic and potassic zones (Figure 13). The models are generated by applying the Datamine studios software and the geological drill core data.

To calculate the spatial correlations between the two binary models, especially the mathematical and geological ones, the logratio matrix [80] can be applied. A comparison between the C-V fractal model results and the geological model of the alteration zones is carried out to obtain the number of overlapped voxels (A, B, C, and D). Using the numbers obtained, Type I error (T1E), Type II error (T2E), and overall accuracy (OA) of different fractal populations are estimated for each one of the alteration zones [92].

According to the C-V fractal modelling result of ANNs, the phyllic alteration zone is correlated with Cu values less than 0.38% (Table 5). By comparing the C-V fractal model thresholds with the alteration zone generated by 3-D geological

modeling, it was found that the Cu values less than 0.38% had more overlapped voxels with OA equal to 0.72.

Comparison between the potassic alteration zones resulting from 3D geological modeling, and the high concentration zones in C-V fractal model shows that Cu values greater than 0.38% with the highest OA (0.71) could recognize the potassic alteration better (Table 6).

One of the most important goals in the exploratory work is the choice of the optimum drilling point to provide a low cost and risk of estimating the mineralization of the area. In Figure 14, a 2D model presenting exploration targets are shown, which could be used to define further drilling sites. For this aim, at first, using the geochemical data at deposit-scale and C-A fractal method, the anomaly's threshold (Cu threshold = 0.1998) was determined and then a prospectivity map (Cu > 0.01998) was drawn. According to the map, further drilling sites should be defined in NW corner of the map.

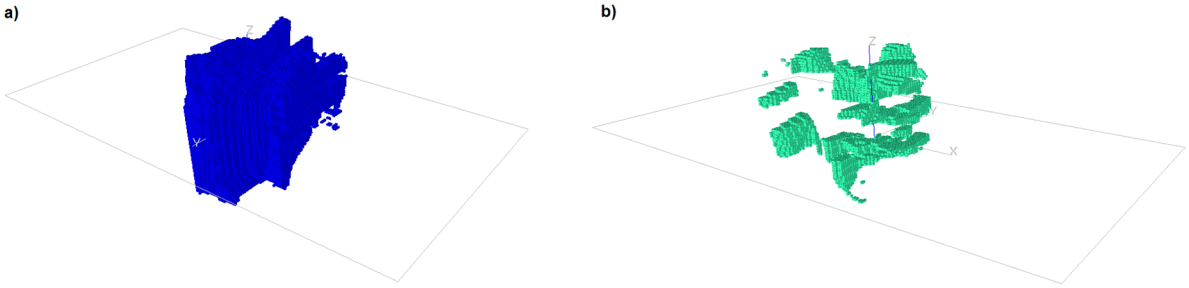

Figure 13. Alteration zones in hypogene zone based on the geological model a) Potassic and b) phyllic alterations.

Table 5. Matrix for calculating spatial correlation between alteration models resulting from C-V fractal modeling and geological model. A and D show the number of voxels that are estimated correctly, and B and C represent the number of voxels with different results in C-V fractal in comparison with the geological model. Overall accuracy (OA), Type I and Type II errors (T1E and T2E, respectively) resulted from the comparison between the phyllic alteration zone in 3D geological model and the first Cu threshold values in the C–V fractal model obtained by ANNs in the hypogene zone.

Geological model					
Fractal model		Inside the zone		outside the zone	
	Inside the model	True positive (A)		False positive (B)	
	Outside the model	False negative (C)		True negative (D)	
		Type I error		Type II error	
		C/(A +C)		B/(B + D)	
		Overall accuracy = (A + D)/(A + B + C + D)			
		Phyllic alteration of geological model			
		Inside the zone		Outside the zone	
Fractal model of areas with low mineralization	Inside the model	A	7829	B	7294
	Outside the model	C	2158	D	17568
		T1E	0.21	T2E	0.30
		OA	0.72		

Table 6. OA, T1E, and T2E resulting from the comparison between the potassic alteration zone in 3D geological model and threshold values of Cu in the C–V fractal model obtained by ANNs in the hypogene zone.

Geological model					
Fractal model		Inside the zone		Outside the zone	
	Inside the model	True positive (A)		False positive (B)	
	Outside the model	False negative (C)		True negative (D)	
		Type I error		Type II error	
		C/(A + C)		B/(B + D)	
		Overall accuracy = (A + D)/(A + B + C + D)			
		Potassic alteration of geological model			
		Inside the zone		Outside the zone	
Fractal model of areas with high mineralization	Inside the model	A	7001	B	3025
	Outside the model	C	1213	D	8143
		T1E	0.14	T2E	0.28
		OA	0.76		

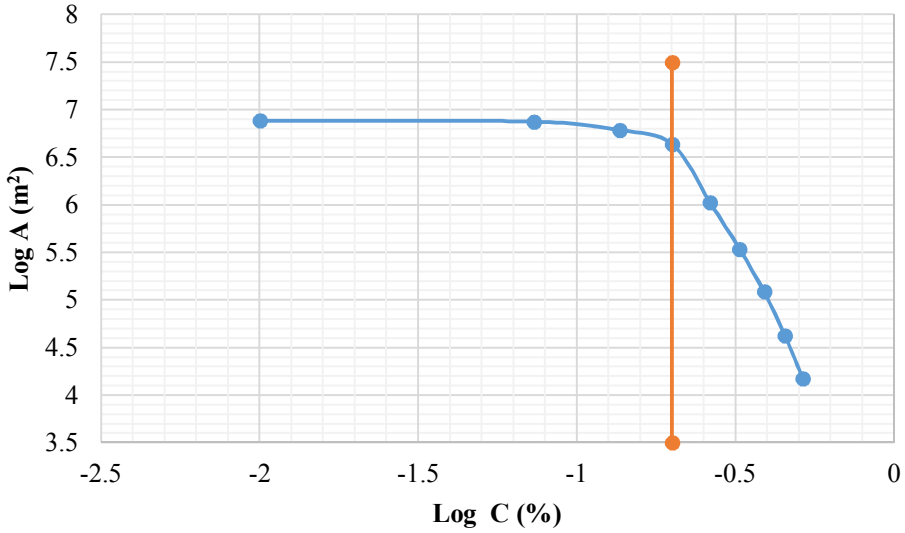

a)

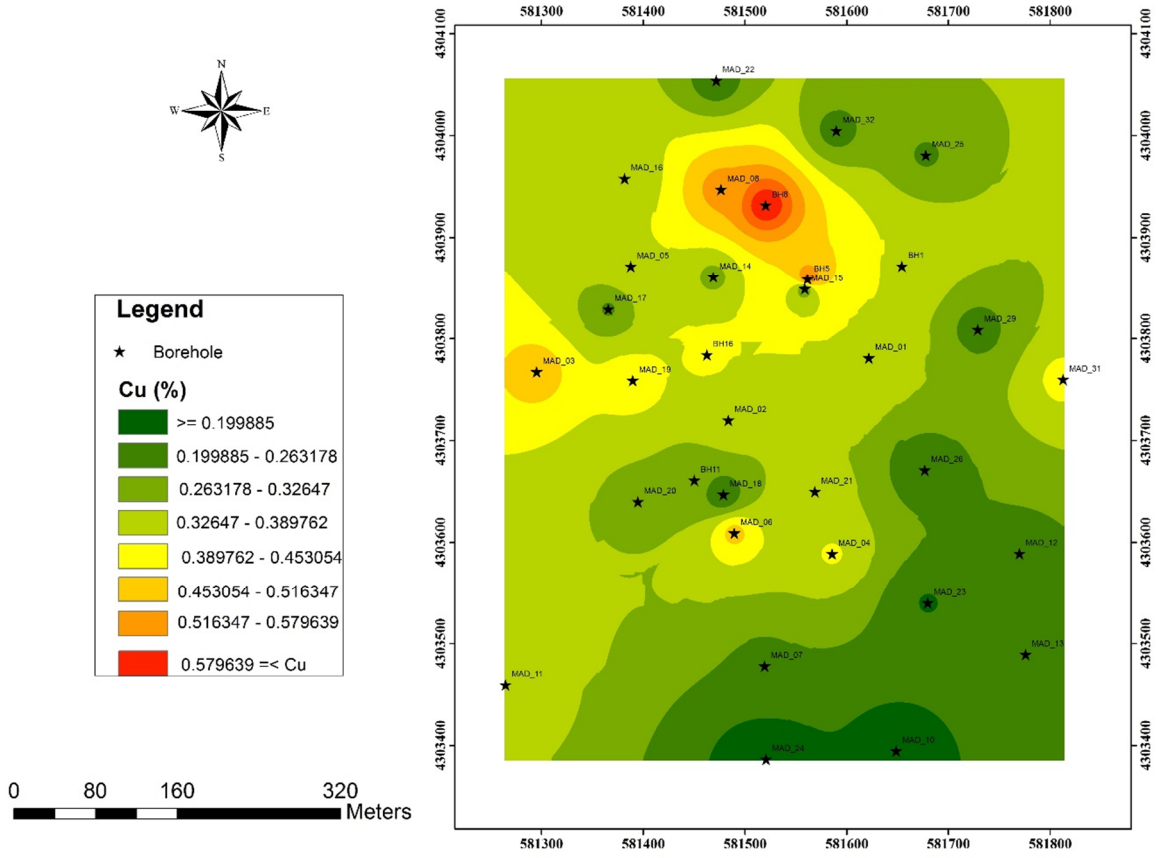

b)

Figure 14. a) Log-Log plot of C-A fractal model, b) a 2D model presenting exploration targets.

6. Conclusions

One of the most important stages in mineral exploration projects is the alteration zone modelling. Alteration modeling is a complicated process, which should be consistent with the geological interpretation. Conventional modeling based on the drill core logging is often descriptive and consists of the uncertainties and lack of the proper recognition of the alteration zones. This type of modeling does not take into account the ore grade, whereas it is a significant variable with an obvious correlation between the alteration

patterns and their distribution. In this work, a combination of ANNs and C-V fractal model was applied to delineate the alteration zones in the hypogene zone of the porphyry copper-gold deposit, Masjed-Daghi, East Azerbaijan Province, Iran. Initially, the efficiency of ANNs was investigated for grade estimation, and the results obtained were compared with OK. The results showed that the kriging algorithm smoothed the data, and thus its application in pre-processing of data for fractal analysis was not conducive. ANNs, which does not require any pre-processing, is known as an alternative in handling such issues. It is not required to carry out variogram operations, and can be used for raw data without any special pre-processing. Secondly, the results obtained from the ANNs estimation along with the concentration-area fractal model were used to delineate the potassic and phyllic alteration areas in the hypogene zone of the Cu-Au porphyry deposit. By comparing the C-V fractal model thresholds with the alteration zone generated by 3-D geological modeling via logratio matrix, it was found that the Cu values less than 0.38% had more overlapped voxels with OA equal to 0.72. Moreover, comparison between the potassic alteration zone resulted from 3D geological modeling, and the high concentration zones in the C-V fractal model showed that Cu values greater than 0.38% with the highest OA (0.71) could recognize potassic alteration better. The overall results showed that the combination of neural network methods and the concentration-area fractal model could be a functional tool for quantitative modeling of the alteration zones instead of the qualitative methods.

References

[1]. Lowell, J.D. and Guilbert, J.M. (1970). Lateral and vertical alteration-mineralization zoning in porphyry ore deposits. Economic Geology. 65: 373-408.

[2]. Soltani, F., Afzal, P. and Asghari, O. (2014). Delineation of alteration zones based on Sequential Gaussian Simulation and concentration–volume fractal modeling in the hypogene zone of Sungun copper deposit, NW Iran. Journal of Geochemical Exploration. 140: 64-76.

[3]. Wilkinson, J.J. (2001). Fluid inclusions in hydrothermal ore deposits. Lithos. 55 (1): 229-272.

[4]. Abbaszadeh, M., Hezarkhani, A. and Soltani-Mohammadi, S. (2013). An SVM-based machine learning method for the separation of alteration zones in Sungun porphyry copper deposit. Chemie der Erde-Geochemistry. 73 (4): 545-554.

[5]. Amer, T.E., El Assay, I.E., Rezk, A.A., El Kammar, A.M., El Manawi, A.W. and Khoziem, H.A. (2014). Geometallurgy and processing of North Ras Mohamed poly-mineralized ore materials, south Sinai, Egypt. Int. J. Miner. Process. 129: 12-21.

[6]. Asghari, O. and Hezarkhani, A. (2008). Appling discriminant analysis to separate the alteration zones within the Sungun porphyry copper deposit. Journal of Applied Sciences. 24: 4472-4486.

[7]. Boisvert, J.B., Rossi, M.E., Ehrig, K. and Deutsch, C.V. (2013). Geometallurgical modeling at Olympic dam mine, South Australia. Math. Geosci. 45 (8): 901-925.

[8]. Lund, C., Lamberg, P. and Lindberg, T. (2013). Practical way to quantify minerals from chemical assays at Malmberget iron ore operations–An important tool for the geometallurgical program. Miner. Eng. 49: 7-16.

[9]. Yildirim, B.G., Bradshaw, D., Powell, M., Evans, C. and Clark, A. (2014). Development of an effective and practical Process Alteration Index (PAI) for predicting metallurgical responses of Cu porphyries. Miner. Eng. 69: 91-96.

[10]. Journel, A.G. and Huijbregts, C.J. (1978). Mining geostatistics. Academic press.

[11]. Rendu, J.M. (1979). Kriging, logarithmic Kriging and conditional expectation: comparison of theory with actual results. Proc., 16th APCOM Symposium. Tucson, Arizona. pp. 199-212.

[12]. Chowdhury, M., Alouani, A. and Hossain, F. (2010). Comparison of ordinary kriging and artificial neural network for spatial mapping of arsenic contamination of groundwater. Stochastic Environmental Research and Risk Assessment. 24 (1): 1-7.

[13]. Chiles, J. P. and Delfiner, P. (2009). Geostatistics: modeling spatial uncertainty. John Wiley & Sons.

[14]. Emery, X. (2005). Simple and ordinary kriging multi-Gaussian kriging for estimating recoverable reserves. Math. Geol. 37: 295-319.

[15]. Emery, X. (2012). Co-simulating total and soluble copper grades in an oxide ore deposit. Math. Geosci. 44 (1): 27-46.

[16]. Maleki Tehrani, M.A., Asghari, O. and Emery, X. (2013). Simulation of mineral grades and classification of mineral resources by using hard and soft conditioning data: application to Sungun porphyry copper deposit. Arab. J. Geosci. 6 (10): 3773-3781.

[17]. Pyrcz, M.J. and Deutsch, C.V. (2014). Geostatistical Reservoir Modeling. Oxford university press.

[18]. Wei, X., Lei, F., Xinye, Z., Pengfei, W., Xiaoli, Y., Xipu, Y. and Jun, L. (2017). Object-based 3D

geomodel with multiple constraints for early Pliocene fan delta in the south of Lake Albert Basin, Uganda. J. Afr. Earth Sci. 125: 1-10.

[19]. Hengl, T. (2009). A practical guide to geostatistical mapping. Vol. 52. 15 P.

[20]. Mpanza, M. (2015). A comparison of ordinary and simple kriging on a PGE resource in the Eastern limb of the Bushveld complex (Doctoral dissertation). 19 P.

[21]. Armstrong, M. (1998). Basic linear geostatistics. Springer Science & Business Media.

[22]. Emery, X. (2005). Simple and ordinary multigaussian kriging for estimating recoverable reserves. Mathematical Geology. 37 (3): 295-319.

[23]. Daya, A.A. (2015). Ordinary kriging for the estimation of vein type copper deposit: A case study of the Chelkureh, Iran. Journal of Mining and Metallurgy A: Mining. 51 (1): 1-14.

[24]. Chilès, J.P. and Delfiner, P. (2012). Geostatistics: Modeling Spatial Uncertainty. Wiley New York.

[25]. Khakestar, M.S., Madani, H., Hassani, H. and Moarefvand, P. (2013). Determining the best search neighbourhood in reserve estimation, using geostatistical method: A case study anomaly No 12A iron deposit in central Iran. Journal of the Geological Society of India. 81 (4): 581-585.

[26]. Strebelle, S. (2002). Conditional simulation of complex geological structures using multiple-point statistics. Mathematical geology. 34 (1): 1-21.

[27]. Reis, A., Sousa, A. and Fonseca, E.C. (2003). Application of geostatistical methods in gold geochemical anomalies identification (Montemor-ONovo, Portugal). Journal of Geochemical Exploration. 77: 45-63.

[28]. Paravarzar, S., Emery, X. and Madani, N. (2015). Comparing sequential Gaussian and turning bands algorithms for cosimulating grades in multi-element deposits. Comptes Rendus Geoscience. 347 (2): 84-93.

[29]. Shahbeik, S., Afzal, P., Moarefvand, P. and Qumarsy, M. (2014). Comparison between Ordinary Kriging (OK) and inverse distance weighted (IDW) based on estimation error. Case study: Dardevey iron ore deposit, NE Iran. Arabian Journal of Geosciences. 7 (9): 3693-3704.

[30]. Tahmasebi, P. and Hezarkhani, A. (2012). A hybrid neural networks-fuzzy logic-genetic algorithm for grade estimation. Computers & geosciences. 42: 18-27.

[31]. Hezarkhani, A. (2008). Hydrothermal evolution of the Miduk porphyry copper system, Kerman, Iran: a fluid inclusion investigation. International Geology Review. 50 (7): 665-684.

[32]. Stöcklin, J. and Setudenia, A. (1972). Lexique Stratigraphique International, Volume III. Paris,

France, ASIE Centre National De La Recherche Scientifique. 75 P.

[33]. Deutsch, C.V. and Journel, A.G. (1998). GSLIB: Geostatistical Software Library and User's Guide. Oxford University Press, New York.

[34]. Journel, A. (1989). Fundamentals of Geostatistics in Five Lessons. American Geophysical Union Publication, Washington, DC. 31 P.

[35]. Denby, B. and Burnett, C. (1993). A neural network based tool for grade estimation, 24th International Symposium on the Application of Computer and Operation Research in the Mineral Industries (APCOM), Montreal, Quebec.

[36]. Singer, D.A. and Kouda, R. (1996). Application of a feedforward neural network in the search for Kuroko deposits in the Hokuroku district, Japan. Mathematical Geology. 28: 1017-1023.

[37]. Koike, K. and Matsuda, S. (2003). Characterizing content distributions of impurities in a limestone mine using a feedforward neural network. Natural resources research. 12: 209-222.

[38]. Porwal, A., Carranza, E. and Hale, M. (2004). A hybrid neuro-fuzzy model for mineral potential mapping. Mathematical geology. 36: 803-826.

[39]. Mahmoudabadi, H., Izadi, M. and Menhaj, M.B. (2009). A hybrid method for grade estimation using genetic algorithm and neural networks. Computational Geosciences. 13: 91-101.

[40]. Xiong, Y. and Zuo, R. (2016). Recognition of geochemical anomalies using a deep autoencoder network. Computers & Geosciences. 86: 75-82.

[41]. Sun, X., Deng, J., Gong, Q., Wang, Q., Yang, L. and Zhao, Z. (2009). Kohonen neural network and factor analysis based approach to geochemical data pattern recognition. Journal of Geochemical Exploration. 103: 6-16.

[42]. Afzal, P., Alghalandis, Y.F., Khakzad, A., Moarefvand, P. and Omran, N.R. (2011). Delineation of mineralization zones in porphyry Cu deposits by fractal concentration–volume modeling. Journal of Geochemical Exploration. 108: 220-232.

[43]. Mandelbrot, B.B. (1982). The fractal geometry of nature. 1982. San Francisco, CA.

[44]. Zhao, J., Chen, S. and Zuo, R. (2016). Identifying geochemical anomalies associated with Au–Cu mineralization using multifractal and artificial neural network models in the Ningqiang district, Shaanxi, China. Journal of Geochemical Exploration. 164: 54-64.

[45]. Zuo, R. (2011). Identifying geochemical anomalies associated with Cu and Pb–Zn skarn

mineralization using principal component analysis and spectrum-area fractal modeling in the Gangdese Belt, Tibet (China). Journal of Geochemical Exploration. 111: 13-22.

[46]. Zuo, R., Cheng, Q., Agterberg, F.P. and Xia, Q. (2009). Evaluation of the uncertainty in estimation of metal resources of skarn tin in Southern China. Ore Geology Reviews. 35: 415-422.

[47]. Liu, H., Wang, Q., Li, G. and Wan, L. (2012). Characterization of multi-type mineralizations in the Wandongshan gold poly-metallic deposit, Yunnan (China), by fractal analysis. Journal of Geochemical Exploration. 122: 20-33.

[48]. Martinez, P., Schertzer, D. and Pham, K. (1997). Texture modelisation by multifractal processes for SAR image segmentation.

[49]. Spirintseva, O.V. (2016). An application of multifractal analysis to photogrammetric image segmentation, Data Stream Mining & Processing (DSMP), IEEE First International Conference on. IEEE. pp. 286-289.

[50]. Daya, A.A. (2015). Application of median indicator kriging in the analysis of an iron mineralization. Arabian Journal of Geosciences. 8: 367-377.

[51]. Li, C., Ma, T. and Shi, J. (2003). Application of a fractal method relating concentrations and distances for separation of geochemical anomalies from background. Journal of Geochemical Exploration. 77: 167-175.

[52]. Zuo, R. (2011). Decomposing of mixed pattern of arsenic using fractal model in Gangdese belt, Tibet, China. Applied Geochemistry. 26: S271-S273.

[53]. Hassanpour, S. and Afzal, P. (2013). Application of concentration–number (C-N) multifractal modeling for geochemical anomaly separation in Haftcheshmeh porphyry system, NW Iran. Arabian Journal of Geosciences. 6: 957-970.

[54]. Berberian, M. and King, G. (1981). Towards a paleogeography and tectonic evolution of Iran. Canadian Journal of Earth Sciences. 18: 210-265.

[55]. Akbarpour, A., Gholami, N., Azizi, H. and Torab, F.M. (2013). Cluster and R-mode factor analyses on soil geochemical data of Masjed-Daghi exploration area, northwestern Iran. Arabian Journal of Geosciences. 6 (9): 3397-3408.

[56]. Farjandi, F., Faiziev, A., Fozilov, M., Bastani, H. and Soleimani, S. (2013). The application of biogeochemistry for gold exploration in the Masjed–Daghi, Julfa, NW Iran. Arabian Journal of Geosciences. 6 (5): 1435-1446.

[57]. Esmaeili, N.A. (2009). Final report of exploration operations in the Cu-Au porphyry ore deposit, Iran National Copper Industry Co. 242 P.

[58]. Dai, F., Zhou, Q., Lv, Z., Wang, X. and Liu, G. (2014). Spatial prediction of soil organic matter content integrating artificial neural network and ordinary kriging in Tibetan Plateau. Ecological Indicators. 45: 184-194.

[59]. Isaaks, E.H. and Srivastava, R.M. (1989). An Introduction to Applied Geostatistics. Oxford University Press, New York. 561 P.

[60]. Krige, D.G. (1951). A statistical approach to some basic mine valuation problems on the Witwatersrand. Journal of the Chemical, 6 Metallurgical and Mining Society. 52: 119-139.

[61]. Matheron, G. (1963). Principles of Geostatistics. Economic Geology. 58: 1246-1266.

[62]. Pokhrel, R.M., Kuwano, J. and Tachibana, S. (2013). A kriging method of interpolation used to map liquefaction potential over alluvial ground. Engineering geology. 152: 26-37.

[63]. Hu, H. and Shu, H. (2015). An improved coarsegrained parallel algorithm for computational acceleration of ordinary Kriging interpolation. Computers & Geosciences. 78: 44-52.

[64]. Vann, J. and Guibal, D. (1998). Beyond Ordinary Kriging-An overview of non-linear estimation, Proceedings of a one day symposium: Beyond Ordinary Kriging.

[65]. Goovaerts, P. (1997). Geostatistics for natural resources evaluation. Oxford University Press on Demand.

[66]. Savory, P.J. (2012). Geostatistical methods for estimating iron, silica and alumina grades within the hardcap of the section seven iron deposit. Tom Price.

[67]. Matheron, G. (1971). The theory of regionalized variables and its application. Les Cahiers du Centre de Morphologie mathematique de Fontainbleau, no. 5, Ecole Nationale Superieure des Mines de Paris.

[68]. Kitanidis, P.K. (1997). Introduction to geostatistics: applications in hydrogeology. Cambridge University Press. pp. 65-74.

[69]. Cressie, N.A.C. (1993). Statistics for Spatial Data. Wiley Series in Probability and Mathematical Statistics: Applied Probability and Statistics. New York: John Wiley & Sons, Inc.

[70]. Wackernagel, H. (2003). Multivariate Geostatistics: An Introduction with Applications (3rd ed.). Berlin, Heidelberg: Springer.

[71]. Webster, R. and Oliver, M.A. (2007). Geostatistics for Environmental Scientists (2nd ed.). Statistics in Practice. Chichester: John Wiley & Sons, Ltd. pp. 155-159.

[72]. Tahmasebi, P. and Hezarkhani, A. (2011). Application of a Modular Feedforward Neural Network

for Grade Estimation. Natural Resources Research. 20: 25-32.

[73]. Samanta, B. and Bandopadhyay, S. (2009). Construction of a radial basis function network using an evolutionary algorithm for grade estimation in a placer gold deposit. Computers & Geosciences. 35 (8): 1592-1602.

[74]. Chatterjee, S., Bhattacherjee, A., Samanta, B. and Pal, S.K. (2006). Ore grade estimation of a limestone deposit in India using an artificial neural network. Applied GIS. 2 (1): 2-1

[75]. Gholamnejad, J., Kasmaee, S., Kohsary, A. and Nezamolhosseini, A. (2012). Grade estimation of ore stockpiles by using Artificial Neural Networks: case study on Choghart Iron Mine in Iran. International Journal of Mining and Mineral Engineering. 4 (1): 17-25.

[76]. Rajasekaran, S. and Pai, G.V. (2003). Neural networks, fuzzy logic and genetic algorithm: synthesis and applications (with cd). PHI Learning Pvt. Ltd. 441 P.

[77]. Szymczyk, P. and Szymczyk, M. (2015). Classification of geological structure using ground penetrating radar and laplace transform artificial neural networks. Neurocomputing. 148: 354-362.

[78]. Van der Baan, M. and Jutten, C. (2000). Neural networks in geophysical applications. Geophysics. 65 (4): 1032-1047.

[79]. Delavar, S.T., Afzal, P., Borg, G., Rasa, I., Lotfi, M. and Omran, N.R. (2012). Delineation of mineralization zones using concentration-volume fractal method in Pb–Zn carbonate hosted deposits. Journal of Geochemical Exploration. 118: 98-110.

[80]. Saein, L.D. (2017). Delineation of enriched zones of Mo, Cu and Re by concentration-volume fractal model in Nowchun Mo-Cu porphyry deposit, SE Iran. iranian journal of earth sciences. 9 (1): 66-74.

[81]. Cousineau, D. and Chartier, S. (2010). Outliers detection and treatment: a review. International Journal of Psychological Research. 3 (1): 58-67.

[82]. Costa, J.F. (2003). Reducing the impact of outliers in ore reserves estimation. Mathematical geology. 35: 323-345.

[83]. Schwertman, N.C., Owens, M.A. and Adnan, R. (2004). A simple more general boxplot method for identifying outliers. Computational statistics & data analysis. 47: 165-174.

[84]. Daya, A.A. (2015). Comparative study of C-A, C-P, and N-S fractal methods for separating geochemical anomalies from background: A case study of Kamoshgaran region, northwest of Iran. Journal of Geochemical Exploration. 150: 52-63.

[85]. Chaturvedi, D., Satsangi, P. and Kalra, P. (1996). Effect of different mappings and normalization of neural network models, Proceedings of the National Power Systems Conference. Indian Institute of Technology. pp. 377-386.

[86]. Sola, J. and Sevilla, J. (1997). Importance of input data normalization for the application of neural networks to complex industrial problems. IEEE Transactions on Nuclear Science. 44: 1464-1468.

[87]. Demuth, H. and Beale, M. (1992). Neural Network Toolbox. For Use with MATLAB. The MathWorks Inc 2000.

[88]. Saljooghi, B.S. and Hezarkhani, A. (2015). A new approach to improve permeability prediction of petroleum reservoirs using neural network adaptive wavelet (wavenet). Journal of Petroleum Science and Engineering. 133: 851-861.

[89]. Kasiviswanathan, K., He, J., Sudheer, K. and Tay, J.H. (2016). Potential application of wavelet neural network ensemble to forecast streamflow for flood management. Journal of Hydrology. 536: 161-173.

[90]. Crochemore, L., Perrin, C., Andréassian, V., Ehret, U., Seibert, S.P., Grimaldi, S., Gupta, H. and Paturel, J.E. (2015). Comparing expert judgement and numerical criteria for hydrograph evaluation. Hydrological Sciences Journal. 60: 402-423.

[91]. Sreekanth, P., Geethanjali, N., Sreedevi, P., Ahmed, S., Kumar, N.R. and Jayanthi, P.K. (2009). Forecasting groundwater level using artificial neural networks. Current science. pp. 933-939.

[92]. Carranza, E.J.M., Zuo, R. and Cheng, Q. (2012). Fractal/multifractal modelling of geochemical exploration data. Journal of Geochemical Exploration. 122: 1-3.

مشخص‌سازی نواحی دگرسانی در زون هیپوژن نهشته پورفیری مس -طلا مسجد داغی، شمال شرق آذربایجان با استفاده از روش‌های شبکه عصبی و فرکتال غلظت- حجم

هانیه نیکوگفتار و اردشیر هزارخانی*

دانشکده مهندسی معدن و متالورژی، دانشگاه صنعتی امیرکبیر، ایران

ارسال ۲۰۱۹/۱/۷، پذیرش ۲۰۱۹/۶/۲۹

* نویسنده مسئول مکاتبات: ardehez@aut.ac.ir

چکیده:

در این پژوهش دو هدف خاص دنبال شده است. نخست، قابلیت تکنیک شبکه عصبی مصنوعی برای تخمین عیار معدنی بررسی شده است. الگوریتم‌های آموزش و تعداد نرون‌های مخفی مختلف برای تخمین عیار مس با داده‌های گمانه‌ای در زون هیپوژن نهشته مس- طلا، مسجد داغی آذربایجان شرقی استفاده شد. کارایی این نوع شبکه عصبی مصنوعی در یادگیری تابع و تخمین عیار با نتایج کریجینگ معمولی مقایسه شد. دوم، نتایج حاصل از تخمین به روش شبکه عصبی مصنوعی به همراه مدل فرکتال غلظت- مساحت برای مشخص‌سازی زون‌های دگرسانی فیلیک و پتاسیک در زون هیپوژن منطقه مورد مطالعه بکار برده شد. برای رسیدن به این مقصود، نخست نمودار لاگ- لاگ بر اساس تخمین به دست آمده از شبکه عصبی تابع پایه شعاعی تولید شد و سپس نقاط شکست این نمودار برای تعیین مقادیر آستانه به منظور مشخص‌سازی زون‌های دگرسانی استفاده شد. به منظور بررسی اعتبار و میزان همبستگی مدل به دست آمده از روش فرکتال غلظت- مساحت و مدل زمین‌شناسی منطقه از ماتریس لگاریتم ریشه‌ای استفاده شد که مقادیر کمتر از ۰/۳۸ درصد عیار دارای بیشترین وکسل‌های همپوشان با زون دگرسانی فیلیک با صحت ۰/۷۲ بودند. بر اساس همبستگی فضایی بین زون دگرسانی پتاسیک منتجه از مدل‌سازی سه‌بعدی زمین‌شناسی و مقادیر غلظت بالا مدل فرکتال غلظت- مساحت نشان داده شده که مقادیر مس بالاتر از ۰/۳۸ با صحت کلی ۰/۷۶ دارای همپوشانی مناسبی با این زون می‌باشند. نتایج به دست آمده نشان داد که ترکیب روش‌های شبکه عصبی و مدل فرکتال غلظت- مساحت می‌تواند یک ابزار مناسب برای مدل‌سازی کمّی زون‌های دگرسانی و در نتیجه مشخص‌سازی سه‌بعدی آن‌ها باشد.

کلمات کلیدی: دگرسانی، شبکه عصبی مصنوعی، مدل فرکتال غلظت- مساحت، نهشته پورفیری مس- طلا مسجد داغی، کریجینگ معمولی.